Atmospheric
Chemistry
and Physics
Discussions

Simulation of the isotopic composition of stratospheric water vapour – Part 1: Description and evaluation of the EMAC model

R. Eichinger[1], P. Jöckel[1], S. Brinkop[1], M. Werner[2], and S. Lossow[3]

[1]Deutsches Zentrum für Luft- und Raumfahrt e.V. (DLR), Institut für Physik der Atmosphäre, Münchner Straße 20, Oberpfaffenhofen, 82234 Weßling, Germany
[2]Alfred Wegener Institute, Helmholtz Centre for Polar and Marine Research, Section Paleoclimate Dynamics, Bussestrasse 24, 27570 Bremerhaven, Germany
[3]Karlsruhe Institute of Technology, Institute for Meteorology and Climate Research, Hermann-von-Helmholtz-Platz 1, 76344 Leopoldshafen, Germany

Correspondence to: R. Eichinger (roland.eichinger@dlr.de)

ACPD

14, 23807–23846, 2014

Simulation of the isotopic composition of stratospheric water vapour – Part 1

R. Eichinger et al.

Title Page

Abstract	Introduction
Conclusions	References
Tables	Figures

| ◄◄ | ►► |
| ◄ | ► |

Back | Close

Full Screen / Esc

Printer-friendly Version

Interactive Discussion

Full Screen / Esc

Abstract

This modelling study aims on an improved understanding of the processes, that determine the water vapour budget in the stratosphere by means of the investigation of water isotope ratios. At first, a separate hydrological cycle has been introduced into the chemistry-climate model EMAC, including the water isotopologues HDO and $H_2^{18}O$ and their physical fractionation processes. Additionally an explicit computation of the contribution of methane oxidation to HDO has been incorporated. The model expansions allow detailed analyses of water vapour and its isotope ratio with respect to deuterium throughout the stratosphere and in the transition region to the troposphere. In order to assure the correct representation of the water isotopologues in the model's hydrological cycle, the expanded system has been evaluated in several steps. The physical fractionation effects have been evaluated by comparison of the simulated isotopic composition of precipitation with measurements from a ground-based network (GNIP) and with the results from the isotopologue-enabled general circulation model ECHAM5-wiso. The model's representation of the chemical HDO precursor CH_3D in the stratosphere has been confirmed by a comparison with chemical transport models (CHEM1D, CHEM2D) and measurements from radiosonde flights. Finally, the simulated stratospheric HDO and the isotopic composition of water vapour have been evaluated, with respect to retrievals from three different satellite instruments (MIPAS, ACE-FTS, SMR). Discrepancies in stratospheric water vapour isotope ratios between two of the three satellite retrievals can now partly be explained.

1 Introduction

30 % of the temperature change since 1980 can be attributed to the radiative forcing of increased stratospheric water vapour (Solomon et al., 2010) and 10 % of the global total ozone decline from 1960 to 1999 can be explained by the water vapour increase (Stenke and Grewe, 2005). However, the mechanisms driving long-term changes in

stratospheric water vapour are not well understood (Füglistaler et al., 2009). Stratospheric water vapour is determined by in situ methane oxidation and the intrusion of water vapour through the tropical tropopause layer (TTL). The seasonal cycle of lower stratospheric water vapour in the tropics is characterised by the tape recorder (Mote et al., 1996), which exhibits a hydrated lower stratosphere in boreal summer and fall and a dry lower stratosphere in boreal winter and spring. Thus, most of the water vapour enters the stratosphere during boreal summer, when the tropopause temperatures are higher and Monsoon systems (e.g. Gettelman and Kinnison, 2004) as well as enhanced deep convection over the tropics (e.g. Khaykin et al., 2009) cause augmented transport of water vapour into the TTL. The contribution of the individual mechanisms on the overall budget of stratospheric water vapour, however, is poorly quantified.

The application of water isotopologues in tracer studies has the potential to answer the open questions, concerning the stratospheric water vapour budget. The different vapour pressures and binding energies of the respective water isotopologues lead to fractionation effects during phase transitions and chemical reactions. The individual processes, which control the water vapour budget in the stratosphere, thus leave an isotopic fingerprint in the respective water vapour compound (Johnson et al., 2001). Direct injection of ice into the stratosphere through deep convection, dehydration of air during ascent by in situ formation of cirrus clouds and the in-mixing of older stratospheric air lead to an offset of the isotope ratios in the upper troposphere and lower statosphere (UTLS) from simple Rayleigh distillation (see Steinwagner et al., 2010). The mechanisms, which are responsible for the intrusion of water vapour into the stratosphere, can hence be separated through the isotopic signature.

Recent satellite retrievals from three different instruments (SMR, MIPAS, ACE-FTS, see Urban et al., 2007; Steinwagner et al., 2007; Nassar et al., 2007) allow to obtain a global picture of the water isotopologue HDO and the water vapour isotope ratio $\delta D(H_2O)$ ($\delta D(H_2O) = \frac{[HDO]/[H_2O]}{R_{VSMOW}}$; ($R_{VSMOW} = 155.76 \cdot 10^{-6}$; Hagemann et al., 1970); VSMOW: Vienna Standard Mean Ocean Water) in the stratosphere and in the transi-

tion region to the troposphere. In some regions the different satellite retrievals, however, show considerable deviations, when comparing profiles and annual cycles of HDO mixing ratios and isotope ratios, respectively (Lossow et al., 2011). Furthermore, Steinwagner et al. (2010) found a tape recorder signal in $\delta D(H_2O)$ in the tropical stratosphere in the MIPAS observations, comparable to the known tape recorder in water vapour mixing ratios. In contrast, Randel et al. (2012) did not find an analogue upward propagation of the seasonal cycle of water vapour isotope ratios in the stratosphere, when analysing ACE-FTS data. Speculations about this discrepancy mainly focus on the different sampling techniques and retrieval algorithms. Consequently, in order to improve the understanding of the basic structure of $\delta D(H_2O)$ in the stratosphere, comprehensive modelling of the physical and chemical isotope processes in a well resolved global chemistry climate model (CCM) with explicit stratospheric dynamics is necessary.

For this purpose, the water isotopologue HDO is here implemented into the EMAC (ECHAM MESSy Atmospheric Chemistry) model (Jöckel et al., 2005, 2010). EMAC provides the opportunity to accurately analyse troposphere-stratosphere exchange processes on a global scale. Depending on the vertical resolution, its base model (ECHAM5; Roeckner et al., 2003) possesses a highly resolved tropopause region (the vertical resolution near the tropopause is about 500 m; see Jöckel et al., 2006) and explicit stratospheric dynamics. Moreover, EMAC includes optional chemical processes, which are needed for the computation of methane oxidation, which is crucial for the representation of H_2O and HDO in the stratosphere. Confirmation of the correct representation of the fractionation processes during phase transitions is achieved through the evaluation of the isotope ratios in precipitation. The consideration of the influence of methane oxidation on atmospheric HDO requires the computation of the methane isotopologue CH_3D. In a next step, this tracer is evaluated with respect to chemical transport models (CHEM1D, CHEM2D, Ridal et al., 2001; Ridal and Siskind, 2002) and measurements from radiosonde flights (Röckmann et al., 2011). At last, the HDO mixing ratios and $\delta D(H_2O)$ in the stratosphere are compared with the observations from satellites. This approach yields a more complete picture of the isotopic composi-

tion of stratospheric water vapour and provides insights into the discrepancies between the respective satellite retrievals. Comprehensive analyses of stratospheric $\delta D(H_2O)$ will be presented in part 2 of this article (Eichinger et al., 2014). Here, the model results will be investigated with respect to the sensitivity and the origin of the $\delta D(H_2O)$ tape recorder and the role of convective ice lofting on the pattern is analysed.

2 Model description and simulation setup

The MESSy-conform submodel H2OISO (H_2O ISOtopologues) has been incorporated into the EMAC model system. This submodel comprises tracers (see Jöckel et al., 2008) for the three stable water isotopologues $H_2^{16}O$ ("normal" water, hereafter denoted as H_2O), $H_2^{18}O$ and HDO for all three phases (vapour, liquid and ice), respectively. Moreover, it contains an additional hydrological cycle, identical to the model's actual hydrological cycle, which includes all processes that modify the tracers and the corresponding fractionation effects for the isotopologues during phase transitions. The modular approach of MESSy allows the optional usage of the H2OISO submodel for all users in future EMAC versions. Besides this structural difference, the implementation of the water isotopologues follows previous studies with ECHAM3 (Hoffmann et al., 1998), ECHAM4 (Werner et al., 2001) and ECHAM5 (Werner et al., 2011). Supplementary to these previous studies, the chemical fractionation effects during the formation of water vapour through methane oxidation were considered. Since observations of water isotopologues in the stratosphere are mostly available for H_2O and HDO, only, the more elaborate accounting for the chemical fractionation of $H_2^{18}O$ was not conducted in this study. Hence, $H_2^{18}O$ basically only serves for the evaluation of the model in the troposphere. The physical isotope effects of HDO and $H_2^{18}O$ only differ by the corresponding fractionation factors.

2.1 Water isotopologues in the hydrological cycle of EMAC

The hydrological cycle in the H2OISO submodel reproduces the actual hydrological cycle of the EMAC model. The tracers for H_2O in the gaseous (H_2O_{vap}), the liquid (H_2O_{liq}) and the ice (H_2O_{ice}) phase were tested to be equal to the standard ECHAM variables for the water vapour (Q), the liquid water (XL) and the ice water (XI) content. Small numerical errors (the maxima are at the order of $10^{-20}\,kg\,kg^{-1}\,s^{-1}$ for water vapour and $10^{-22}\,kg\,kg^{-1}\,s^{-1}$ for liquid water and ice), which arise due to the coding design, are corrected after each time step, in order to prevent the two hydrological cycles from diverging. Moreover, we assured that these numerical errors are small enough to not deteriorate the calculation of the water isotopologues.

For the water isotopologues, fractionation effects occur during phase changes. Equilibrium and kinetic fractionation during the evaporation of water from oceans is described by the bulk formula by Hoffmann et al. (1998). The surface flux for the water isotopologues depends on the isotope ratio of the ocean, the wind speed above the surface, the sea surface temperature, the specific humidity and the isotopic composition of the vapour above the surface (Hoffmann et al., 1998). As in the study by Werner et al. (2011), the isotope ratio of the ocean is prescribed with a global gridded data set based on the ^{18}O isotopic composition in sea water by LeGrande and Schmidt (2006). Since there is no equivalent data set for the deuterium isotopic composition, the HDO content is prescribed with eight times the $H_2^{18}O$ mixing ratios. This is in accordance with global observations (Craig and Gordon, 1965). Due to the limitations of the applied land surface scheme in the EMAC model, we neglect any isotope fractionation from land surfaces. The land surface scheme in EMAC is identical to the scheme in the ECHAM5 model. A more detailed description of this simplification is given in Werner et al. (2011). As for water vapour, liquid water and ice in the actual hydrological cycle, the advection of the new water isotopologue tracers follows the flux form semi-Lagrangian (FFSL) scheme by Lin and Rood (1996).

The cloud and convection parameterisation routines (CLOUD and CONVECT) in EMAC include a number of phase transitions and therefore several different fractionation effects. Again, the implementation follows the study of Werner et al. (2011). During the formation of clouds, condensation of water vapour to liquid water and deposition of vapour to cloud ice take place. For condensation within clouds, a closed system is assumed. The condensate is taken on to be in contact, and hence in isotopic equilibrium, with the surrounding vapour during the entire process. This also applies for the evaporation of cloud water, where, in contrast to evaporation from the ocean, a closed system is assumed. An open system is used for the deposition of water vapour to ice. Due to the low diffusivities of the isotopologues in the ice phase, no exchange happens between ice and vapour. The effective fractionation factor α_{eff} is used here, including a function for the supersaturation S. Werner et al. (2011) adjusted this function to $S = 1.01 - 0.0045 \cdot T_{\text{cond}}$ (with T_{cond} as the condensation temperature, given in °C), in order to attain realistic isotope ratios in Antarctic snow. Since the focus of the present study lies on the tropopause region, where also low temperatures have a major effect on kinetic fractionation through deposition, as a first estimate, the values from Werner et al. (2011) have been taken. During the melting of ice and the freezing of water, no fractionation is assumed. Other in-cloud processes like sedimentation of ice, autoconversion, accretion and aggregation include no fractionation effects either. The isotopic (non-)equilibrium factor α_{eff}, which describes a fractionation process between a falling raindrop and the surrounding water vapour, may vary with time. Its value depends on the humidity, the temperature, the diffusivity of the water molecules and the droplet size. Since these processes are not resolved in GCMs, the fractionation during reevaporation of raindrops falling through undersaturated air can only be approximated. Following Hoffmann et al. (1998), an isotopical equilibration of 45 % is assumed for large drops from convective rain and 95 % for small drops falling from stratiform clouds. Due to their low exchange rates, snow and ice do not reequilibrate at all, which leads to more depleted isotope ratios in solid precipitation.

2.2 Stratospheric isotope chemistry for water and methane

The EMAC model contains the submodel CH4, which provides a simplified methane oxidation mechanism to take into account the chemical production of water vapour. It includes a tracer for methane (the CH_4 tracer), which experiences a source from the surface (here as lower boundary conditions from the submodel TNUDGE, see next section; alternatively as methane fluxes, provided by the submodel OFFEMIS, see Jöckel et al., 2010) and a sink in form of methane oxidation. Solutions are calculated for the four oxidation reactions, which are determined by the mixing ratios of the three oxidation partners (Cl, OH, O(^{1}D)) and the photolysis rate. The photolysis rate j_{CH_4}(= $r_{h\nu}$) is here calculated in the MESSy submodel JVAL (for details, see Landgraf and Crutzen, 1998) and passed on to CH4 (alternatively it can be prescribed). The rates for the oxidation of methane with the reaction partners Cl, OH and O(^{1}D) are calculated within CH4. First, the first order reaction coefficients k_{OH} for OH, k_{Cl} for Cl and k_{O1D} for O(^{1}D) are determined. While $k_{O1D} = 1.75 \cdot 10^{-10}\,cm^3\,s^{-1}$ is constant, k_{OH} and k_{Cl} are temperature (T in K) dependent and are computed by

$$k_{OH} = 1.85 \cdot 10^{-20} \cdot \exp\left(2.82 \cdot \log(T) - \frac{987}{T}\right)\,cm^3\,s^{-1} \tag{1}$$

and

$$k_{Cl} = 6.6 \cdot 10^{-12} \cdot \exp\left(-\frac{1240}{T}\right)\,cm^3\,s^{-1}. \tag{2}$$

Subsequently the rates for the reactions with methane are

$$r_{O1D} = k_{O1D} \cdot c_{air} \cdot O(^1D) \tag{3}$$
$$r_{Cl} = k_{Cl} \cdot c_{air} \cdot Cl \tag{4}$$
$$r_{OH} = k_{OH} \cdot c_{air} \cdot OH, \tag{5}$$

with O(^{1}D), Cl and OH representing the prescribed mixing ratios (in mol mol^{-1}) of the respective species and c_{air} the concentration of dry air molecules (in cm^{-3}), which is calculated by

$$c_{air} = \frac{N_A \cdot 10^{-6} \cdot p}{R_{gas} \cdot T \cdot \left[1 + \left(\frac{M_{air}}{M_{H_2O}} - 1\right) \cdot Q\right]}.$$ (6)

Here N_A denotes the Avogadro Constant ($6.022045 \cdot 10^{23}$ mol^{-1}), p the pressure (in Pa), R_{gas} the universal gas constant (8.314409 J K^{-1} mol^{-1}), T the temperature (in K), M_{air} the molar mass of dry air (28.97 g mol^{-1}), M_{H_2O} the molar mass of water (18.02 g mol^{-1}) and Q the specific humidity (in kg kg^{-1}).
The tendency for the methane tracer (in mol mol^{-1} s^{-1}) is then given by

$$\frac{\partial(CH_4)}{\partial t} = -1 \cdot CH_4 \cdot (r_{O1D} + r_{Cl} + r_{OH} + r_{hv}),$$ (7)

where CH_4 is the methane mixing ratio (in mol mol^{-1}) of the previous time step and the -1 accounts for the fact that this is a pure sink reaction for the methane tracer. To calculate the tendency for the specific humidity due to methane oxidation,

$$\left.\frac{\partial Q}{\partial t}\right|_C = \frac{-2 \cdot \frac{\partial(CH_4)}{\partial t}}{\frac{M_{air}}{M_{H_2O}} \left(\frac{1}{1-Q}\right)^2}$$ (8)

is applied. The subscript C denotes, that this is the chemical tendency of Q. This division is to convert the tendency from mol mol^{-1} s^{-1} to kg kg^{-1} s^{-1}. The negative sign here accounts for the fact that methane oxidation is a source for water vapour and the factor 2 for the reaction of the four hydrogen atoms of one methane molecule into two water molecules.

In order to take into account the chemical production of HDO, analogously a parameterisation for the oxidation of CH_3D has been devised. A tracer for CH_3D, the most abundant deuterium isotopologue of methane, was included for this purpose. The coefficients for the mass-dependent kinetic isotope effects (KIE) for the reactions of CH_3D with OH, $O(^1D)$ and Cl have been determined in laboratory measurements by Saueressig et al. (1996, 2001). They are partly temperature dependent and can be described with the function $KIE(T) = A \cdot \exp(B/T)$. The values for A and B and their temperature ranges are given in Table 1 (see also Röckmann et al., 2011). The absorption cross-section of CH_3D is shifted 0.9 nm blueward relative to CH_4 (Nair et al., 2005). For the photodissociation of CH_3D, this results in the fractionation factor $KIE_{h\nu} = 0.995$ in the atmosphere of Mars (see also Nixon et al., 2012). This approach is here applied onto the Earth's atmosphere, since the photodissociation characteristics of methane do not differ from one planet of the solar system to another.

As for physical kinetic fraction processes, the Rayleigh equation

$$R = R_0 \left(\frac{N}{N_0} \right)^{KIE^{-1}-1} \tag{9}$$

is applied for the fractionation processes in the chemical reactions. Inserting the isotope ratios (R_0 and R) and the total mixing ratios (N_0 and N) before and after the reaction, leads to

$$\frac{CH_3D - \frac{\partial(CH_3D)}{\partial t}}{CH_4 - \frac{\partial(CH_4)}{\partial t}} = \frac{CH_3D}{CH_4} \left(\frac{CH_4 - \frac{\partial(CH_4)}{\partial t}}{CH_4} \right)^{KIE^{-1}-1}. \tag{10}$$

Title Page

Abstract | Introduction

Conclusions | References

Tables | Figures

◀ | ▶

◀ | ▶

Back | Close

Full Screen / Esc

Printer-friendly Version

Interactive Discussion

Using Eq. (7) for $\partial(CH_4)/\partial t$ and considering that the KIE is different for each of the reactions, the tendency of the CH_3D tracer is given by

$$\frac{\partial(CH_3D)}{\partial t} = CH_3D \cdot \left[\left(1 - (1 + r_{OH})^{KIE_{OH}^{-1}}\right) + \left(1 - (1 + r_{Cl})^{KIE_{Cl}^{-1}}\right) + \right.$$
$$\left. \left(1 - (1 + r_{O1D})^{KIE_{O1D}^{-1}}\right) + \left(1 - (1 + r_{hv})^{KIE_{hv}^{-1}}\right) \right]. \tag{11}$$

In order to calculate the tendency of the HDO tracer from the tendency of the CH_3D tracer (i.e. the chemical tendency of HDO), analogously to Eq. (8),

$$\left.\frac{\partial(HDO)}{\partial t}\right|_C = \frac{-1 \cdot \frac{\partial(CH_3D)}{\partial t}}{\frac{M_{air}}{M_{HDO}} \left(\frac{1}{1-HDO}\right)^2}, \tag{12}$$

is applied. Here, we use the specific humidity and the molar mass of HDO (M_{HDO} = 19.02 g mol^{-1}) instead of Q and M_{H_2O} and the factor 1 instead of 2, because the oxidation of one CH_3D molecule can only produce one HDO molecule.

This simple parameterisation, however, neglects a number of effects that may be important for the chemical production of HDO: firstly, the other, rather rare methane isotopologues CH_2D_2, CHD_3 and CD_4 as well as the reaction partner OD (an isotopologue of the hydroxyl radical) are not considered. Secondly, the entire cycle of molecular hydrogen and its isotopologue HD is not taken into consideration. The intermediate reactions between CH_3D and HDO involving HD also include fractionation effects (see e.g. Röckmann et al., 2003; Rhee et al., 2006). Most of these, however, are poorly quantified (Zahn et al., 2006) and therefore neglected for this initial study. These simplifications have to be kept in mind when evaluating the model results in the stratosphere. Emissions of CH_3D could be defined with the aid of an extension (for deuterium) of the MESSy isotope scheme of Gromov et al. (2010). However, this task goes beyond the scope of our study, which mainly focuses on stratospheric and upper tropospheric processes. This leads to another simplification: in accordance with

Ridal and Siskind (2002) the isotope ratio of methane was fixed to −68‰ in the tropo-sphere (i.e. here, below 500 hPa). This is within the range of the climatological $\delta D(CH_4)$ ($\delta D(CH_4)$ is also based on VSMOW) value, which methane possesses when entering the stratosphere in the tropics, derived from measurements by Irion et al. (1996).

2.3 Simulation setup

For this study, an EMAC (v2.42) model simulation, in T42L90MA resolution was per-formed. This corresponds to an approximate horizontal grid box size of 2.8° × 2.8°, 90 vertical layers and explicitly resolved stratospheric dynamics. The uppermost model layer is centered around 0.01 hPa. The MESSy submodels, which were applied in this simulation (in addition to the described H2OISO and CH4 submodels and the ECHAM5 base model from EMAC version 2.42) are listed and described in the ap-pendix. The time step of the simulation was twelve minutes and the output was set to produce instantaneous values with an interval of eleven hours. The EMAC model pro-vides the possibility to use several different convection schemes. In all the simulations conducted for this study, the "Tiedtke–Nordeng" convection scheme (Tiedtke, 1989) was applied. Before starting the actual simulation, a 20 year free running simulation was carried out to obtain steady-state initial values for water, methane and their iso-topologues. From these initial conditions a simulation with specified dynamics (i.e. in "nudged" mode) was started, which means a Newtonian relaxation of the divergence, the vorticity, the temperature and the logarithm of the surface pressure towards refer-ence data. Here, the relaxation is performed up to 1 hPa towards the ERA-INTERIM reanalysis data (ECMWF; Dee et al., 2011). This guarantees, that not only the climatic state, but also the meteorological situation of the model simulation corresponds to the actual states and allows a direct comparison of the model results with satellite or in situ measurements. The simulation starts at the beginning of the year 1982 and terminates at the end of the year 2011. From the steady-state conditions, which are used for the initialisation, the model again needs several years to adjust to the conditions of the "nudged" mode. The first eight years are hence not considered for the analysis. Only

the 21 years from 1990 until 2011 are evaluated. Transient greenhouse gas concentrations are prescribed throughout the atmosphere. Methane is prescribed at the lower boundary through the submodel TNUDGE, based on observations. The mixing ratios of OH, Cl, O(^{1}D) are prescribed (monthly averages) from a previous "nudged", transient EMAC simulation with full chemistry. The same applies for ozone, which is needed to calculate the photolysis rate in the submodel JVAL. As mentioned above, the methane oxidation is calculated in the CH4 submodel.

3 Model evaluation

Before evaluating the model simulation with respect to the isotopic composition of water vapour in the stratosphere, we show that the basis for this is established in the EMAC model. This includes the correct representation of the physical water isotope effects in the troposphere and the chemical HDO precursor CH_3D in the stratosphere, as well as its sink reactions. Subsequently stratospheric HDO mixing ratios and $\delta D(H_2O)$ are compared to satellite observations.

3.1 Water isotope ratios in precipitation

The isotopic composition in precipitation allows to conclude various fractionation processes (Dansgaard, 1964). Hence, the representation of the isotope physics in the model can be evaluated by examining the isotope ratios in precipitation. This has been conducted in many studies with isotopologue-enabled GCMs (e.g. Risi et al., 2010; Werner et al., 2011).

The GNIP (Global Network of Isotopes in Precipitation) measurement survey provides a comprehensive data base for this purpose. The International Atomic Energy Agency (IAEA) and the World Meteorological Organisation (WMO) have started GNIP in 1961. Since its start, more than 800 meteorological stations in 101 countries have collected samples of the water isotopologues HDO and $H_2^{18}O$ in precipitation

(IAEA/WMO, 2006). Some of these stations provided monthly precipitation measurements for several decades, most of them, however, operated for a much shorter period, only. This data set serves as a basis for the evaluation of the simulated isotope ratios in the troposphere. Good qualitative agreement was achieved when comparing the general global patterns in annual mean precipitation, as well as in the seasonal cycles between GNIP and EMAC. Details can be found in the Supplement.

The isotopologue-enabled GCM ECHAM5-wiso (water isotopologues) has also been tested successfully against GNIP data, as well as against other water isotopologue measurements (see Werner et al., 2011). Several model resolutions have been applied for this study. The results of the lowest of these horizontal resolutions (T31 $\sim 3.75° \times 3.75°$) was largely reproduced with the EMAC model (see Supplement). Since the model physics and dynamics of the two models, including the hydrological cycle and the implementation of the water isotopologues (as described in Sect. 2), are almost identical, this is not surprising. However, it is a prerequisite for assuring the correct representation of the tropospheric isotope composition of water. A detailed comparison between EMAC and ECHAM5-wiso is given in the Supplement. The good quantitative agreement of this comparison supports the conclusion, that the EMAC model with the H2OISO submodel represents the state of the art of GCMs with an explicit representation of the water isotopologues HDO and $H_2^{18}O$ in the troposphere.

3.2 CH$_3$D in the stratosphere

The simulated CH$_3$D is compared to results from the CHEM1D model by Ridal et al. (2001) and the CHEM2D model by Ridal and Siskind (2002). These models comprise an oxidation scheme, where CH$_3$D produces HDO through a number of chemical reactions. This oxidation scheme was developed for the CHEM1D model. For the CHEM2D model, it was extended for higher altitudes and included into the Naval Research Laboratory two-dimensional chemical/dynamical model. In Ridal (2002) and Ridal and Siskind (2002) the two chemical transport models have shown good general agreement with measurements from the ATMOS (Atmospheric Trace MOlecule Spec-

troscopy) instrument (Irion et al., 1996). ATMOS provides global data for CH_3D and HDO, however, with large uncertainties. The averaged equatorial values of $\delta D(CH_4)$ of EMAC, CHEM2D and CHEM1D are presented in Fig. 1.

Since in all three models, the tropospheric values of $\delta D(CH_4)$ are fixed (−68‰ in EMAC and CHEM2D, −65‰ in CHEM1D), they do not differ below the tropopause. Moreover, the overall dependence of $\delta D(CH_4)$ on altitude qualitatively agrees in all the three model simulations. Between 20 and 50 km altitude the methane isotope ratio increases from −68‰ to around +120‰ in CHEM2D and CHEM1D, and to around +130‰ in EMAC. Especially the increase in the lower stratosphere is much stronger in EMAC, which leads to rather large discrepancies in the altitude range between 30 and 40 km. Between 50 and 60 km, both, CHEM2D and EMAC, show almost no change in $\delta D(CH_4)$ with altitude, CHEM1D does not extend above 50 km. This is the transition region between the altitudes of the chemical and the photolytic methane oxidation. The photodissociation, which becomes important above 60 km and increases continuously above, is much stronger in CHEM2D at first. This is somewhat surprising, because there is no fractionation included for the photolysis of CH_3D in the CHEM2D model. Even though the fractionation for photolysis in EMAC is very small, the photolysis of CH_3D is expected to be of similar strength as in CHEM2D. The discrepancy is hence likely caused by the differences in the calculation of the photolysis rates in EMAC and CHEM2D. Since the mid of the uppermost layer of the EMAC model in the applied resolution is at 80 km, a comparison further above is not possible.

Measurements of CH_3D in the stratosphere are sparse. Röckmann et al. (2011), however, collected 13 samples from stratospheric balloon borne air measurements, which were provided by the Max-Planck Institute (MPI) for Solar System Research and by the Institute for Atmospheric and Environmental Sciences of the University of Frankfurt. The mixing ratios and the isotopic composition of CH_4 were measured, using a high-precision continuous flow isotope ratio mass spectrometry system (Brass and Röckmann, 2010). Twelve of these balloon flights can be used for direct intercomparison with the data from the EMAC simulation. One flight (Flight ID: HYD-87-03) was

conducted in 1987. Since the model results are considered to be in steady-state only from 1990 on, this sample is not taken into account for the evaluation. In Fig. 2, twelve panels are presented, with the balloon borne data and the EMAC results of $\delta D(CH_4)$ with altitude, between 5 and 35 km. The flight IDs, included in the panels provide infor-

5 mation about the location, the month and the year of the balloon flights (see caption). To provide an estimate about the average and the annual variability of $\delta D(CH_4)$ in the model simulation, additionally, the averages, maxima and minima of the 21 simulation years of the respective months at the location of the launch are included in the panels.

    In general, good qualitative agreement can be observed between the measured

10 and the simulated data. Both simulation and measurements, show an increase of the methane isotope ratios from tropospheric values to values between −100‰ and −200‰ at 25 to 35 km in the Arctic region and to values between 0 and −100‰ in the mid-latitude and tropical regions. The balloon borne samples are mostly lying within the extremes of the simulation and close to the simulated values from the same day and

15 location. The measured values in the troposphere and lower stratosphere, however, are systematically lower than the simulated values. In contrast to the −68‰ for strato-spheric entry values of $\delta D(CH_4)$, suggested by Ridal and Siskind (2002); Röckmann et al. (2011) assess the typical tropospheric $\delta D(CH_4)$ value to be −81‰. This explains the constant offset at lower altitudes between the two data sets and, it adjusted, is

20 also expected to reduce the differences at higher altitudes. However, since firstly, as Ridal and Siskind (2002) we focus on the stratospheric entry values of $\delta D(CH_4)$ in the inner tropics and secondly, this uncertainty at these altitudes has only little rele-vance for the HDO mixing ratios, we did not perform this adjustment. The simulated steep increase of $\delta D(CH_4)$ above 25 to 30 km can only be seen in the measurements

25 in the Arctic region (KIR). The mid-latitude (GAP and ASA) samples show large de-viations at these altitudes. The differences in the profiles of the KIR-00-01 and the KIR-03-03 samples between simulation and balloon flights are exceptional. Apart from the lower stratospheric regions (and the values above 25 km in sample KIR-03-03) the measured $\delta D(CH_4)$ values are constantly higher than the simulated values. These

Title Page

Abstract   Introduction

Conclusions   References

Tables   Figures

|◄   ►|

◄   ►

Back   Close

Full Screen / Esc

Printer-friendly Version

Interactive Discussion

two samples are associated with special meteorological and thus chemical situations. The KIR-03-03 sample comprises a mesospheric enclosure and during the sampling of the KIR-00-01 data, a strong Arctic vortex was present (Röckmann et al., 2011). These phenomena can also be observed in the simulation, due to the "nudging" these

5 special meteorological situations and the associated chemical situations are broadly represented. However, the horizontal resolution of the model simulation is too coarse, to resolve sharp horizontal gradients around the site of the balloon launch. Also, the balloons drift off the launching site while ascending can cause deviations of such magnitudes.

10 Another method for evaluating the methane isotope chemistry is assessing the relation of $\delta D(CH_4)$ to the CH_4 mixing ratio. The $\delta D(CH_4)$ values of the same data as in Fig. 2, from 5 to 35 km altitude, are plotted vs. the CH_4 mixing ratios in Fig. 3. The figure is divided into the launches in the polar region (KIR) in the left panel and the launches in mid- (ASA, GAP) and tropical (HYD) latitudes in the right panel.

15 Again a constant offset between the simulation and the measurements can be seen. Apart from a single exception (the measurement from the HYD-99-04 sample, right panel) the simulated $\delta D(CH_4)$ values are generally higher for the same methane mixing ratios. Decreasing the fixed tropospheric value can reduce this offset. The slope of increasing isotope ratios with decreasing methane mixing ratios is in very good

20 agreement. Since these compact tracer-tracer correlations are generally found for trace gases whose life times are longer than the transport times (Plumb and Ko, 2004), it implies that the chemical removal of the CH_3D tracer in relation to the removal of the CH_4 tracer, is well represented, despite the simplified chemistry parameterisation.

3.3 HDO in the stratosphere

25 During the first decade of the 21st century, three satellite missions collected data, applicable for the retrieval of the water isotopologue HDO in the stratosphere. The MIPAS (Michelson Interferometer for Passive Atmospheric Sounding) instrument on Envisat (Environmental Satellite) allowed the retrieval of HDO by measuring the thermal emis-

sion in the mid-infrared. This high-resolution Fourier transform spectrometer measured at the atmospheric limb and provided data for HDO retrievals in full spectral resolution from July 2002 to March 2004, roughly in the altitude range between 10 and 50 km. It orbits the Earth sun-synchronously 14 times a day. The vertical resolution for the retrieval of HDO is around 5 km between the tropopause and 30 km altitude, above it degrades ($\sim$ 8 km at 40 km) (Steinwagner et al., 2007; Lossow et al., 2011). The Odin satellite also orbits the Earth sun-synchronously and carries the SMR (Sub-Millimetre Radiometer) instrument, among other purposes to passively measure HDO on the global scale roughly on one day per week. It operates in the microwave range. Data has been retrieved from the start of the mission in 2001 until today, at altitudes between roughly 20 and 70 km with a vertical resolution of around 3 km (Urban et al., 2007). The ACE-FTS (Atmospheric Chemistry Experiment Fourier Transform Spectrometer) instrument circularly orbits the Earth on the SCISAT satellite and obtains Fourier transform absorption spectra from solar occultation measurements. It has a vertical resolution between 2 and 6 km and a comparably limited spatial sampling. The ACE orbit is optimised for measurements in mid- and high latitudes, the tropics are only covered during the four months of February, April, August and October (Nassar et al., 2007; Randel et al., 2012).

Lossow et al. (2011) collected data of the three instruments for intercomparison and concluded a good consistency between MIPAS and ACE-FTS at altitudes above 20 km. Below this altitude, issues like different cloud filtering and measurement techniques as well as different vertical resolutions cause large deviations. Generally, in the stratosphere the MIPAS and the ACE-FTS data agree favourably, the SMR data shows considerably dryer conditions, especially below 30 km. This is mainly due to uncertainties in the different spectroscopies of the instruments (Lossow et al., 2011).

These data could now also be used to evaluate the HDO simulated by EMAC. In Fig. 4, the tropical (15° S to 15° N) values of the HDO mixing ratios of the three satellite instruments and the EMAC model are presented. Additionally to the data of MIPAS, SMR and version 2.2 of ACE-FTS shown by Lossow et al. (2011), here also version

3.0 of ACE-FTS is included, which reaches higher up in the stratosphere, compared to version 2.2. Since ACE-FTS only provides data for four months per year in this region, the panels show averages for February, April, August and October. Since the years of the ACE-FTS and the MIPAS satellite retrievals do not overlap, a direct comparison is not possible. However, tests have shown, that the averages of the periods of the individual retrievals do not show substantial differences between each other and between the average of the entire simulation. In order to get a good estimate for the comparison of the model with all retrievals and for the annual variability, the averages, the minima and the maxima of the respective months have been taken from the entire 21 years of the EMAC simulation.

The EMAC data is generally dryer in HDO compared to the MIPAS and the ACE-FTS profiles in each of the presented months at all altitudes. Only between 30 and 35 km the HDO profiles of EMAC increase stronger than in the satellite data and reach the level of MIPAS and ACE-FTS HDO mixing ratios. In the altitude range between 16 and 30 km the EMAC simulation quantitatively corresponds well with the Odin retrieval. In this region also local maxima and minima, which can be seen in all four satellite profiles are reproduced qualitatively in EMAC. These reveal the seasonal cycle of HDO. However, especially for April and August, the local minimum between 25 and 30 km in the EMAC data is not as pronounced as in the satellite retrievals. Above 40 km the HDO mixing ratios of all satellite profiles increase strongly with altitude to values around 1.1 nmol mol^{-1} at 50 km, while the EMAC simulation shows HDO mixing ratios of only 0.9 nmol mol^{-1} at these altitudes. This is most likely due to the assumptions made in the chemistry parameterisation, which does not include the influence of the isotopic composition of molecular hydrogen on HDO.

3.4 The stratospheric δD tape recorder

The tape recorder signal in H_2O, HDO and $\delta D(H_2O)$ in the EMAC simulation is evaluated with respect to the MIPAS data. The satellite and the model data are compared

in Fig. 5. The left panels show the EMAC results and the right panels show the MIPAS retrieval.

Overall, there is only a rather weak agreement between EMAC and MIPAS in all three quantities. A persistent (all altitudes, all seasons) dry bias in H_2O and HDO is visible in the EMAC simulation. This offset has also been shown by Jöckel et al. (2006) and is consistent with the slightly too cold hygropause in the nudging data (see e.g. Liu et al., 2010). $\delta D(H_2O)$ is slightly too high in the upper stratosphere and generally too low in the lower stratosphere. In the lower stratosphere, some of these differences can be explained with the coarse vertical resolution of the MIPAS retrieval, which smoothes the hygropause (see Steinwagner et al., 2007). The overestimation of $\delta D(H_2O)$ in EMAC at around 35 km corresponds to the altitudes ($\sim$ 30–35 km), where HDO increases more strongly in the simulation, as seen in Fig. 4. In the lower stratosphere, the strongest deviations in $\delta D(H_2O)$ can be observed during NH summer, when MIPAS observations show $\delta D(H_2O)$ values around –500‰ and the $\delta D(H_2O)$ values in EMAC do not exceed –600‰. A tape recorder signal can be seen in all three quantities for both, model and observations, although with different amplitudes and a phase shift of two to three months. While the maxima of the tape recorder in the lower stratosphere in EMAC are found during summer, the satellite data show them at the beginning of autumn. This can partly be an artefact of the MIPAS retrieval and its vertical sampling, but has to be kept in mind and compared with other data sets. The tape recorder signals in HDO and H_2O fade out at around 30 km in both, model and observations. The $\delta D(H_2O)$ tape recorder signal in MIPAS reaches these altitudes as well, the EMAC $\delta D(H_2O)$ tape recorder, in contrast, fades out below 25 km already.

The amplitude of the tape recorder in EMAC is larger for H_2O and smaller for HDO and $\delta D(H_2O)$, respectively, compared to the MIPAS data. Above 25 km, the $\delta D(H_2O)$ tape recorder becomes overshadowed by chemically produced high $\delta D(H_2O)$ values. This effect is further investigated in part 2 of the article (Eichinger et al., 2014). The MIPAS $\delta D(H_2O)$ tape recorder might be amplified artificially by the offsets in vertical

Title Page

Abstract	Introduction
Conclusions	References
Tables	Figures

|◀ | ▶|

◀ | ▶

Back | Close

Full Screen / Esc

Printer-friendly Version

Interactive Discussion

resolution between H_2O and HDO (Orbe et al., 2013). A correction of this error is likely to reveal a $\delta D(H_2O)$ tape recorder signal with smaller amplitude in the MIPAS retrieval.

By analysing ACE-FTS data, Randel et al. (2012) found a tape recorder signal in H_2O and in HDO, but could not find a corresponding pattern in $\delta D(H_2O)$. The lower stratosphere in Fig. 7 of Randel et al. (2012) shows distinct seasonally varying maxima and minima of $\delta D(H_2O)$, these, however, hardly propagate upwards in time. For comparison with the ACE-FTS data, the tropical H_2O, HDO and $\delta D(H_2O)$ in the stratosphere of the EMAC simulation are displayed in Fig. 6 for the same period as in Randel et al. (2012).

The left panels show the monthly averages of the respective values. Quantitatively these agree fairly well with the ACE-FTS observations by Randel et al. (2012). The increase of the quantities with altitude in the stratosphere is represented well. At 30 km $\delta D(H_2O)$ exhibits values around −500‰, which matches with ACE-FTS data. Similarly to the comparison with the MIPAS retrieval, however, the lower stratosphere in EMAC is dryer, especially in HDO. Still, a clear tape recorder signal can be observed in all three panels, with minimum values in the lower stratosphere during boreal winter and maxima during boreal summer.

For the right panels, the EMAC data has been filtered, using only the four months (February, April, August and October), which are also available in the ACE-FTS retrieval, to estimate the influence of the sparse temporal sampling on the tape recorder signals. This filtering somewhat blurs the tape recorder in all three panels, compared to the full data set. Especially the tape recorder in $\delta D(H_2O)$, however, appears to lose some of its upward motion at around 20 km and generally becomes less obvious. Therefore, it can be assumed, that the sparse temporal sampling of ACE-FTS data is an issue in the evaluation of the $\delta D(H_2O)$ tape recorder and may well contribute to the indistinctness of the signal in the study by Randel et al. (2012).

Due to its instrumental design, the SMR satellite instrument measures H_2O and HDO orbitally shifted. This means, that H_2O and HDO are never measured at the same time

and implies inaccuracies for the calculation of $\delta\text{D}(\text{H}_2\text{O})$. A comparison of the $\delta\text{D}(\text{H}_2\text{O})$ tape recorder signal between EMAC and SMR has therefore not been conducted.

3.5 Summary and discussion

The results of the EMAC simulations were first assessed with respect to the isotope ratios in precipitation, in order to ensure the correct representation of the physical processes in the troposphere. The EMAC results agree very well with GNIP (IAEA/WMO, 2006) data and are almost identical with results from the ECHAM5-wiso (Werner et al., 2011) model. Hence the physical processes and fractionation effects of the water isotopologues in the hydrological cycle of EMAC are represented satisfactorily.

The chemical HDO precursor CH_3D in the stratosphere was evaluated next. Here, a good qualitative agreement with chemically elaborate transport models by Ridal et al. (2001) and Ridal and Siskind (2002), as well as with radiosonde flights by Röckmann et al. (2011) is shown. Quantitative differences can merely be speculated about. Differences in the model dynamics as well as in the fractionation coefficients can play a role in the model-model intercomparison. The climatological value of tropospheric $\delta\text{D}(\text{CH}_4)$, the coarse horizontal resolution of the model, the possible drift of the balloon and associated local meteorological features and especially the sparsity of the measurements are the main issues in the comparison of $\delta\text{D}(\text{CH}_4)$ in EMAC with observations. As desired by Röckmann et al. (2011), this modelling approach can assist for further studies, especially concerning the investigation of the isotope effects of the chemical sink reactions of methane isotopologues. Anyhow, more extensive measurements are desired for further evaluation of the methane isotope ratios in the stratosphere.

The mixing ratios of HDO were compared with satellite retrievals. Inconsistencies between the individual satellite retrievals (see Lossow et al., 2011) make it delicate to define a distinct result. In the UTLS, the HDO profiles of EMAC agree well with the SMR satellite retrieval. Compared to the ACE-FTS and the MIPAS satellite profiles, retrieved from measurements in the mid-infrared, the UTLS appears to be too dry in HDO in the EMAC model. A possible explanation for this, however, also is the lack of the

representation of ice overshooting convection in the here applied convection scheme (Tiedtke–Nordeng; Tiedtke, 1989). According to Dessler et al. (2007), a more complete representation of this effect can enhance the mixing ratios of HDO, while H_2O is not significantly affected. The rather low vertical resolution of the satellite observations, on the other hand, blur the hygropause. Hence, the HDO mixing ratios at the tropopause might be overestimated (see e.g., Steinwagner et al., 2007). Between 30 and 35 km the simulated HDO increases stronger with altitude than the satellite observations show. This is most likely to be a chemical effect, since it is obvious during all the four months where observations of ACE-FTS are available. This can be linked to the fractionation factors in the sink reaction of CH_3D, because also $\delta D(CH_4)$ is overestimated at these altitudes, especially in the tropical and mid-latitude profiles. A revision of the applied kinetic fractionation parameters and their temperature dependence (which were taken from Röckmann et al., 2011), is necessary to analyse this offset. The HDO mixing ratios above 40 km are underestimated by the EMAC model. This is attributable to the lack of the intermediate reactions containing HD in the CH_3D oxidation chain in the model, which include isotope effects. As has been shown by Röckmann et al. (2003), strato-spheric $\delta D(H_2)$ increases with altitude, while the mixing ratio of molecular hydrogen is rather constant. Additionally, the influence of the oxidation of CH_3D itself also increases with altitude. This implies, that the intermediate reaction with HD on HDO, which is not implemented here, increases with altitude too. That simplification can therefore explain the offset in HDO mixing ratios between the EMAC simulation and the satellite retrievals above 40 km.

In future studies, the chemical deficiencies of the H2OISO submodel can be re-duced, by including a representation of HD to take into account the intermediate reac-tions from CH_3D to HDO. However, according to Zahn et al. (2006) the reaction rates of HD and especially the fractionation effects of these reactions are poorly quantified and hence can be subject of large uncertainties. As an alternative, however more so-phisticated modelling approach, the water isotopologues can be included to the isotope scheme by Gromov et al. (2010), by extending it to the deuterium cycle. This features

Title Page

Abstract | Introduction

Conclusions | References

Tables | Figures

|◄ | ►|

◄ | ►

Back | Close

Full Screen / Esc

Printer-friendly Version

Interactive Discussion

a number of isotopic species and reactions, which also affect the hydrogen reactions. Furthermore, the usage of other convection schemes may generate more suitable results of HDO in the UTLS. This, however, requires the implementation of the water isotopologues into the alternative convection schemes.

The tape recorder signals of H_2O, HDO and $\delta D(H_2O)$ of the EMAC simulation were compared to the MIPAS retrieval (see Steinwagner et al., 2007, 2010). In the lower stratosphere, EMAC and MIPAS are closest during winter, where the differences can mostly be explained with the low vertical resolution of the MIPAS sampling. The summer months, however, show much stronger deviations between model and observations, with too low values in all quantities in the simulation. This suggests deficiencies in the model physics, most likely the underrepresentation of overshooting convection. Furthermore, a hardly explainable phase shift and, especially in $\delta D(H_2O)$, inconsistent amplitudes and vertical propagations between the tape recorder signals are observed. The inconsistent vertical resolutions between H_2O and HDO in the MIPAS retrieval can be the reason of an amplification of the $\delta D(H_2O)$ tape recorder signal in the observations. The correction of this artefact in the MIPAS data is subject of current investigations and may lead to more consistency in the amplitudes of the $\delta D(H_2O)$ recorders between EMAC and MIPAS.

The seasonal cycle of lower stratospheric $\delta D(H_2O)$ in the ACE-FTS retrieval (see Randel et al., 2012) shows a different behaviour than that of the MIPAS retrieval and the EMAC simulation. The too low HDO mixing ratios in EMAC compared to ACE-FTS, especially during summer, are consistent, however, Randel et al. (2012) can not find the tape recorder signal in $\delta D(H_2O)$. The $\delta D(H_2O)$ tape recorder in EMAC is weaker than the corresponding signals in H_2O and HDO. Still, the pattern is clearly recognisable in the lower stratosphere. A possible reason for the lack of the upward propagation of the seasonal cycle of $\delta D(H_2O)$ in the ACE-FTS observations is the sparse temporal sampling of the instrument in the tropics. A filtering of the EMAC data to its sampling reduces the apparent temporal upward motion of the $\delta D(H_2O)$ tape recorder in the lower stratosphere and the signal fades out at even lower altitudes. In fact, this filtering

makes the δD(H$_2$O) tape recorder hardly recognisable and therewith more similar to the ACE-FTS retrieval.

In order to constitute more quantitative comparisons between models and observations, more sophisticated methods will be applied in future evaluations. The vertical resolution of the EMAC data can be transformed to the resolution of the respective satellite retrieval using their averaging kernel. Also, the cloud filtering methods used for the satellite data can be applied onto the model data. This elaborate evaluation can possibly assist to reduce the discrepancies between model results and observations and reveal the model's and the measurement's insufficiencies more precisely. In this study, however, a more comprehensive understanding of the δD(H$_2$O) tape recorder is desired, which can best be achieved with the complete data record.

4 Conclusions

The EMAC model system has been extended with the submodel H2OISO, which contains a separate hydrological cycle, comprising the water isotopologues HDO and H$_2^{18}$O and their physical fractionation effects. The good agreement with measurement data and the ECHAM5-wiso model lead to the conclusion, that this expanded model system represents the state of the art of water isotopologue-enabled atmosphere GCMs. Moreover, a parameterisation of the oxidation of CH$_3$D was included to the H2OISO submodel. The sink reactions of CH$_3$D, which include reaction- and partly temperature-dependent kinetic fractionation effects, determine the chemical production of HDO. This rather simple parameterisation for the methane isotopologue CH$_3$D is apparently quite robust and can be applied for further studies concerning the isotopic composition of methane in the stratosphere. The comparison of stratospheric HDO profiles with satellite observations reveals a qualitatively good agreement. In some regions, however, systematic discrepancies can be observed. These can be associated with uncertainties in the convection scheme, the kinetic fractionation coefficients in the chemical reactions and the simplified reaction chain, which does not consider molecular hydrogen.

The comparison of the stratospheric tape recorder signal in H_2O, HDO and $\delta D(H_2O)$ between EMAC and satellite observations is difficult. Considering all the uncertainties in the measurements and in the model, the overall representations of the tape recorder signals in EMAC are reasonable. The $\delta D(H_2O)$ tape recorder simulated by EMAC at least partly resolves the discrepancies between the divergent conclusions from the MIPAS and the ACE-FTS satellite retrievals. The EMAC $\delta D(H_2O)$ tape recorder ranges between the pronounced tape recorder from MIPAS and the missing upward propagation of the seasonal signal in ACE-FTS observations. The revision of the individual insufficiencies of the retrievals, however, are expected to alter the observations towards the EMAC results. Despite the quantitative differences in stratospheric $\delta D(H_2O)$ between EMAC and satellite observations, the conclusion can be drawn, that the new MESSy submodel H2OISO, used in the framework of the EMAC model, provides the possibility to attain additional insights into the mechanisms, which control the stratospheric water vapour budget. The physical and chemical properties of the isotopic composition of water allow new investigation measures, with respect to the processes and pathways, which control the stratospheric water vapour budget. The H2OISO submodel will be available in future EMAC versions as an additional option for all users.

Appendix A: Applied MESSy submodels

- CLOUD: original **cloud** and cover routines from ECHAM5 as MESSy submodel (Roeckner et al., 2006, and references therein).

- CONVECT: this submodel calculates the process of **Convect**ion. It consists of an interface to choose different convection schemes and the calculations themselves (Tost et al., 2006).

- CVTRANS: the **C**on**v**ective **T**racer T**rans**port submodel calculates the transport of tracers due to convection. It uses a monotonic, positive definite and mass conserving algorithm following the bulk approach (Tost, 2006).

- – GWAVE: Hines non-orographic **g**ravity **wave** routines from ECHAM5 as MESSy submodel (Roeckner et al., 2006).

- – RAD4ALL: ECHAM5 radiation scheme as MESSy submodel (Roeckner et al., 2006; Jöckel et al., 2006).

- – TROPOP: submodel for **Tropop**ause (WMO + PV) and other diagnostics (Jöckel et al., 2006).

- – JVAL: this submodel is for fast online calculation of **J-val**ues (photolysis rate co-efficients) using cloud water content and cloudiness calculated by the base model and/or climatological ozone and climatological aerosol (based on Landgraf and Crutzen, 1998).

- – TNUDGE: the submodel "**T**racer **Nudg(e)**ing" is used for Newtonian relaxation of user-defined tracers as pseudo-emissions (Kerkweg et al., 2006).

The Supplement related to this article is available online at doi:10.5194/acpd-14-23807-2014-supplement.

Title Page

Abstract | Introduction

Conclusions | References

Tables | Figures

|◄ | ►|

◄ | ►

Back | Close

Full Screen / Esc

Printer-friendly Version

Interactive Discussion

References

Brass, M. and Röckmann, T.: Continuous-flow isotope ratio mass spectrometry method for carbon and hydrogen isotope measurements on atmospheric methane, Atmos. Meas. Tech., 3, 1707–1721, doi:10.5194/amt-3-1707-2010, 2010. 23821

Craig, H. and Gordon, L. I.: Deuterium and oxygen 18 variations in the ocean and the marine atmosphere, in: Stable Isotopes in Oceanographic Studies and Paleotemperatures, edited by: Lischi, V., Pisa, Italy, 9–130, 1965. 23812

Dansgaard, W.: Stable isotopes in precipitation, Tellus, 16, 436–468, 1964. 23819

Dee, D. P., Uppala, S. M., Simmons, A. J., Berrisford, P., Poli, P., Kobayashi, S., Andrae, U., M. A. Balmaseda, M. A., Balsamo, G., Bauer, P., Bechtold, P., Beljaars, A. C. M., van de Berg, L., Bidlot, J., Bormann, N. B., Delsol, C., Dragani, R., Fuentes, M., Geer, A. J., Haimberger, L., Healy, S. B., Hersbach, H., Hólm, E. V., Isaksen, L., Kållberg, P., Köhler, M., Matricardi, M., McNally, A. P., Monge-Sanz, B. M., Morcrette, J.-J., Park, B.-K., Peubey, C., de Rosnay, P., Tavolato, C., Thépaut, J.-N., and Vitart, F.: The ERA-Interim reanalysis: configuration and performance of the data assimilation system, Q. J. Roy. Meteor. Soc., 656, 553–597, 2011. 23818

Dessler, A. E., Hanisco, T. F., and Füglistaler, S.: Effects of convective ice lofting on H_2O and HDO in the tropical tropopause layer, J. Geophys. Res.-Atmos., 112, D18309, doi:10.1029/2007JD008609, 2007. 23829

Eichinger, R., Jöckel, P., and Lossow, S.: Simulation of the isotopic composition of stratospheric water vapour – Part 2: Investigation of HDO/H_2O variations, Atmos. Chem. Phys. Discuss., in preparation, 2014. 23811, 23826

Füglistaler, S., Dessler, A. E., Dunkerton, J. T., Folkins, I., Fu, Q., and Mote, P. W.: Tropical Tropopause Layer, Rev. Geophys., 47, RG1004, doi:10.1029/2008RG000267, 2009. 23809

Gettelman, A. and Kinnison, D. E.: Impact of monsoon circulations on the upper troposphere and lower stratosphere, J. Geophys. Res., 109, D22101, doi:10.1029/2004JD004878, 2004. 23809

Gromov, S., Jöckel, P., Sander, R., and Brenninkmeijer, C. A. M.: A kinetic chemistry tagging technique and its application to modelling the stable isotopic composition of atmospheric trace gases, Geosci. Model Dev., 3, 337–364, doi:10.5194/gmd-3-337-2010, 2010. 23817, 23829

Title Page

Abstract | Introduction

Conclusions | References

Tables | Figures

◄ | ►

◄ | ►

Back | Close

Full Screen / Esc

Printer-friendly Version

Interactive Discussion

Hagemann, R., Nief, G., and Roth, E.: Absolute isotopic scale for deuterium analysis of natural waters, Absolute D/H ratio for SMOW, Tellus, 22, 712–715, 1970. 23809

Hoffmann, G., Werner, M., and Heimann, M.: Water isotope module of the ECHAM atmospheric general circulation model: a study on timescales from days to several years, J. Geophys. Res., 103, 16871–16896, 1998. 23811, 23812, 23813

IAEA/WMO: Global Network of Isotopes in Precipitation: The GNIP Database, International Atomic Energy Agency, available at: http://www-naweb.iaea.org/napc/ih/IHS_resources_gnip.html, Last access date: 15.09.2014, 2006. 23820, 23828

Irion, F. W., Moyer, E. J., Gunson, M. R., Rinsland, C. P., Yung, Y. L., Michelsen, H. A., Salawitch, R. J., Chang, A. Y., Newchurch, M. J., Abbas, M. M., Abrams, M. C., and Zander, R.: Stratospheric observations of CH_3D and HDO from ATMOS infrared solar spectra: enrichments of deuterium in methane and implications for HD, Geophys. Res. Lett., 23, 2381–2384, 1996. 23818, 23821

Jöckel, P., Sander, R., Kerkweg, A., Tost, H., and Lelieveld, J.: Technical Note: The Modular Earth Submodel System (MESSy) – a new approach towards Earth System Modeling, Atmos. Chem. Phys., 5, 433–444, doi:10.5194/acp-5-433-2005, 2005. 23810

Jöckel, P., Tost, H., Pozzer, A., Brühl, C., Buchholz, J., Ganzeveld, L., Hoor, P., Kerkweg, A., Lawrence, M. G., Sander, R., Steil, B., Stiller, G., Tanarhte, M., Taraborrelli, D., van Aardenne, J., and Lelieveld, J.: The atmospheric chemistry general circulation model ECHAM5/MESSy1: consistent simulation of ozone from the surface to the mesosphere, Atmos. Chem. Phys., 6, 5067–5104, doi:10.5194/acp-6-5067-2006, 2006. 23810, 23826, 23833

Jöckel, P., Kerkweg, A., Buchholz-Dietsch, J., Tost, H., Sander, R., and Pozzer, A.: Technical Note: Coupling of chemical processes with the Modular Earth Submodel System (MESSy) submodel TRACER, Atmos. Chem. Phys., 8, 1677–1687, doi:10.5194/acp-8-1677-2008, 2008. 23811

Jöckel, P., Kerkweg, A., Pozzer, A., Sander, R., Tost, H., Riede, H., Baumgaertner, A., Gromov, S., and Kern, B.: Development cycle 2 of the Modular Earth Submodel System (MESSy2), Geosci. Model Dev., 3, 717–752, doi:10.5194/gmd-3-717-2010, 2010. 23810, 23814

Johnson, D. G., Jucks, K. W., Traub, W. A., and Chance, K. V.: Isotopic composition of stratospheric water vapor: Implications for transport, J. Geophys. Res., 106, 12219–12226, 2001. 23809

Kerkweg, A., Sander, R., Tost, H., and Jöckel, P.: Technical note: Implementation of prescribed (OFFLEM), calculated (ONLEM), and pseudo-emissions (TNUDGE) of chemical species in the Modular Earth Submodel System (MESSy), Atmos. Chem. Phys., 6, 3603–3609, doi:10.5194/acp-6-3603-2006, 2006. 23833

Khaykin, S., Pommereau, J.-P., Korshunov, L., Yushkov, V., Nielsen, J., Larsen, N., Christensen, T., Garnier, A., Lukyanov, A., and Williams, E.: Hydration of the lower stratosphere by ice crystal geysers over land convective systems, Atmos. Chem. Phys., 9, 2275–2287, doi:10.5194/acp-9-2275-2009, 2009. 23809

Landgraf, J. and Crutzen, P. J.: An efficient method for online calculations of photolysis and heating rates, J. Atmos. Sci., 55, 863–878, 1998. 23814, 23833

LeGrande, A. N. and Schmidt, G. A.: Global gridded data set of the oxygen isotopic composition in seawater, Geophys. Res. Lett., 33, L12604, doi:10.1029/2006GL026011, 2006. 23812

Lin, S. J. and Rood, R. B.: Multidimensional flux form semi-Lagrangian transport, Mon. Weather Rev., 124, 2046–2068, 1996. 23812

Liu, Y. S., Fueglistaler, S., and Haynes, P. H.: Advection-condensation paradigm for stratospheric water vapor, J. Geophys. Res., 115, D24, doi:10.1029/2010JD014352, 2010. 23826

Lossow, S., Steinwagner, J., Urban, J., Dupuy, E., Boone, C. D., Kellmann, S., Linden, A., Kiefer, M., Grabowski, U., Glatthor, N., Höpfner, M., Röckmann, T., Murtagh, D. P., Walker, K. A., Bernath, P. F., von Clarmann, T., and Stiller, G. P.: Comparison of HDO measurements from Envisat/MIPAS with observations by Odin/SMR and SCISAT/ACE-FTS, Atmos. Meas. Tech., 4, 1855–1874, doi:10.5194/amt-4-1855-2011, 2011. 23810, 23824, 23828

Mote, P., Rosenlof, K., McIntyre, M., Carr, E., Gille, J., Holton, J., Kinnersley, J., Pumphrey, H., Russel, J., and Waters, J.: An atmospheric tape recorder: the imprint of tropical tropopause temperatures on stratospheric water vapor, J. Geophys. Res., 101, 3989–4006, 1996. 23809

Nair, H., Summers, M. E., Miller, C. E., and Yung, Y. L.: Isotopic fractionation of methane in the martian atmosphere, Icarus, 175, 32–35, 2005. 23816

Nassar, R., Bernath, P. F., Boone, C. D., Gettelman, A., McLeod, S. D., and Rinsland, C. P.: Variability in HDO/H_2O abundance ratios in the tropical tropopause layer, J. Geophys. Res., 112, D21305, doi:10.1029/2007JD008417, 2007. 23809, 23824

Nixon, C. A., Temelso, B., Vinatier, S., Teanby, N. A., Bézard, B., Achterberg, R. K., Mandt, K. E., Sherrill, C. D., Irwin, P. G. J., Jennings, D. E., Romani, P. N., Coustenis, A., and Flasar, F. M.: Isotopic ratios in Titan's methane: measurements and modelling, Astrophys. J., 749, 159 (15pp), doi:10.1088/0004-637X/749/2/159, 2012. 23816

Title Page

Abstract | Introduction

Conclusions | References

Tables | Figures

|◀ | ▶|

◀ | ▶

Back | Close

Full Screen / Esc

Printer-friendly Version

Interactive Discussion

Orbe, C., Garny, H., and Seviour, W.: SPARC Workshop on the Brewer–Dobson Circulation, SPARC Newsletter, No. 40, 11–21, 2013. 23827

Plumb, R. A. and Ko, M. K. W.: Interrelationships between mixing ratios of long lived stratospheric constituents, J. Geophys. Res., 101, 3957–3972, 2004. 23823

Randel, W. J., Moyer, E., Park, M., Jensen, E., Bernath, P., Walker, K., and Boone, C.: Global variations of HDO and HDO/H_2O ratios in the upper troposphere and lower stratosphere derived from ACE-FTS satellite measurments, J. Geophys. Res., 117, D06303, doi:10.1029/2011JD016632, 2012. 23810, 23824, 23827, 23830, 23846

Rhee, T. S., Brenninkmeijer, C. A. M., Braß, M., and Brühl, C.: Isotopic composition of H_2 from CH_4 oxidation in the stratosphere and the troposphere, J. Geophys. Res., 111, D23303, doi:10.1029/2005JD006760, 2006. 23817

Ridal, M.: Isotopic ratios of water vapor and methane in the stratosphere: comparison between ATMOS measurements and a one-dimensional model, J. Geophys. Res., 107, D164285, doi:10.1029/2001JD000708, 2002. 23820

Ridal, M. and Siskind, D. E.: A two-dimensional suimulation of the isotopic composition of water vapor and methane in the upper atmosphere, J. Geophys. Res., 107, D244807, doi:10.1029/2002JD002215, 2002. 23810, 23818, 23820, 23822, 23828, 23841

Ridal, M., Jonsson, A., Werner, M., and Murtagh, D. P.: A one-dimensional simulation of the water vapor isotope HDO in the tropical stratosphere, J. Geophys. Res., 106, 32283–32294, 2001. 23810, 23820, 23828, 23841

Risi, C., Bony, S., Vimeux, F., and Jouzel, J.: Water-stable isotopes in the LMDZ4 general circulation model: model evaluation for present-day and past climates and applications to climatic interpretations of tropical isotopic records, J. Geophys. Res., 115, D12118, doi:10.1029/2009JD013255, 2010. 23819

Röckmann, T., Rhee, T. S., and Engel, A.: Heavy hydrogen in the stratosphere, Atmos. Chem. Phys., 3, 2015–2023, doi:10.5194/acp-3-2015-2003, 2003. 23817, 23829

Röckmann, T., Brass, M., Borchers, R., and Engel, A.: The isotopic composition of methane in the stratosphere: high-altitude balloon sample measurements, Atmos. Chem. Phys., 11, 13287–13304, doi:10.5194/acp-11-13287-2011, 2011. 23810, 23816, 23821, 23822, 23823, 23828, 23829, 23840, 23842

Roeckner, E., Bäuml, G., Bonaventura, L., Brokopf, R., Esch, M., Giorgetta, M., Hagemann, S., Kirchner, I., Kornblueh, L., Manzini, E., Rhodin, A., Schlese, U., Schulzweida, U., and Tomp-

kins, A.: The Atmospheric General Circulation Model ECHAM 5. Part I: Model Description., Report No. 349, Max-Planck-Institut für Meteorologie, Hamburg, 2003. 23810

Roeckner, E., Brokopf, R., Esch, M., Giorgetta, M., Hagemann, S., Kornblueh, L., Manzini, E., Schlese, U., and Schulzweida, U.: Sensitivity of simulated climate to horizontal and vertical resolution in the ECHAM5 atmosphere model, J. Climate, 19, 3771–3791, 2006. 23832, 23833

Saueressig, G., Bergamaschi, P., Crowley, J., Fischer, H., and Harris, G.: D/H kinetic isotope effects in the reaction $CH_4 + Cl$, Geophys. Res. Lett., 23, 3619–3622, 1996. 23816

Saueressig, G., Crowley, J., Bergamaschi, P., Brühl, C., Brenninkmeijer, C., and Fischer, H.: Carbon 13 and D kinetic isotope effects in the reactions of CH_4 with $O(^1D)$ and OH: new laboratory measurements and their implications for the isotopic composition of stratospheric methane, J. Geophys. Res., 106, 23127–23138, 2001. 23816

Solomon, S., Rosenlof, K. H., Portmann, R. W., Daniel, J. S., Davis, S. M., Sanford, T. J., and Plattner, G.-K.: Contributions of stratospheric water vapor to decadal changes in the rate of global warming, Science, 327, 1219–1223, 2010. 23808

Steinwagner, J., Milz, M., von Clarmann, T., Glatthor, N., Grabowski, U., Höpfner, M., Stiller, G. P., and Röckmann, T.: HDO measurements with MIPAS, Atmos. Chem. Phys., 7, 2601–2615, doi:10.5194/acp-7-2601-2007, 2007. 23809, 23824, 23826, 23829, 23830

Steinwagner, J., Füglistaler, S., Stiller, G., von Clarmann, T., Kiefer, M., Borsboom, P.-P., van Delden, A., and Röckmann, T.: Tropical dehydration processes constrained by the seasonality of stratospheric deuterated water, Nat. Geosci., 3, 262–266, doi:10.1038/NGEO822, 2010. 23809, 23810, 23830

Stenke, A. and Grewe, V.: Simulation of stratospheric water vapor trends: impact on stratospheric ozone chemistry, Atmos. Chem. Phys., 5, 1257–1272, doi:10.5194/acp-5-1257-2005, 2005. 23808

Tiedtke, M.: A comprehensive mass flux scheme for cumulus parameterization in large-scale models, Mon. Weather Rev., 117, 1779–1800, 1989. 23818, 23829

Tost, H.: Global Modelling of Cloud, Convection and Precipitation Influences on Trace Gases and Aerosols, PhD thesis, University of Bonn, Germany, 2006. 23832

Tost, H., Jöckel, P., and Lelieveld, J.: Influence of different convection parameterisations in a GCM, Atmos. Chem. Phys., 6, 5475–5493, doi:10.5194/acp-6-5475-2006, 2006. 23832

Urban, J., Lautié, N., Murtagh, D., Eriksson, P., Kasai, Y., Lossow, S., Dupuy, E., de La Noë, J., Frisk, U., Olberg, M., Le Flochmoën, E., and Ricaud, P.: Global observations of middle atmo-

Title Page

Abstract | Introduction

Conclusions | References

Tables | Figures

|◄ | ►|

◄ | ►

Back | Close

Full Screen / Esc

Printer-friendly Version

Interactive Discussion

spheric water vapour by the Odin satellite: an overview, Planet. Space Sci., 55, 1093–1102, 2007. 23809, 23824

Werner, M., Heimann, M., and Hoffmann, G.: Isotopic composition and origin of polar precipitation in present and glacial climate simulations, Tellus B, 53, 53–71, 2001. 23811

5 Werner, M., Langebroek, P. M., Carlsen, T., Herold, M., and Lohmann, G.: Stable water isotopes in the ECHAM5 general circulation model: Toward high-resolution isotope modeling on a global scale, J. Geophys. Res., 116, D15109, doi:10.1029/2011JD015681, 2011. 23811, 23812, 23813, 23819, 23820, 23828

Zahn, A., Franz, P., Bechtel, C., Grooß, J.-U., and Röckmann, T.: Modelling the budget of middle

10 atmospheric water vapour isotopes, Atmos. Chem. Phys., 6, 2073–2090, doi:10.5194/acp-6-2073-2006, 2006. 23817, 23829

R. Eichinger et al.

Full Screen / Esc

Printer-friendly Version

Interactive Discussion

Table 1. Temperature dependent kinetic isotope fractionation coefficients for the reaction with CH_3D. The kinetic isotope effect is determined by $KIE(T) = A \cdot \exp(B/T)$ for the given temperature range (see Röckmann et al., 2011).

Reactant	T range	A	B
OH		1.097	49 ± 22
O(^{1}D)	224–295	1.066	0
Cl	223–295	1.278	51.31 ± 19.1
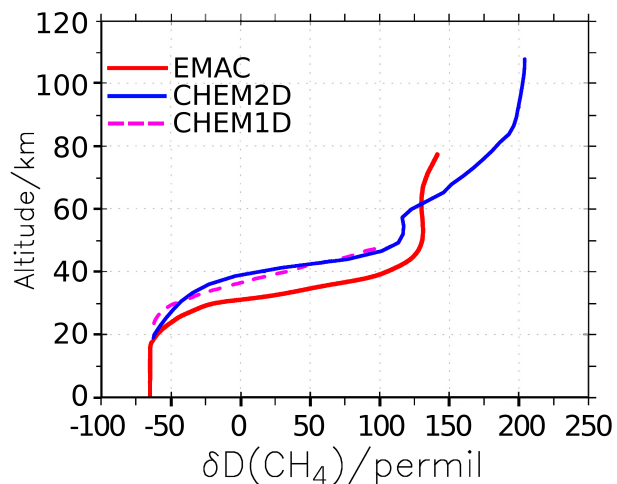
Figure 1. Comparison of equatorial averages of $\delta D(CH_4)$ with altitude between EMAC (red), CHEM2D (blue) by Ridal and Siskind (2002) and CHEM1D (dashed purple) by Ridal et al. (2001).
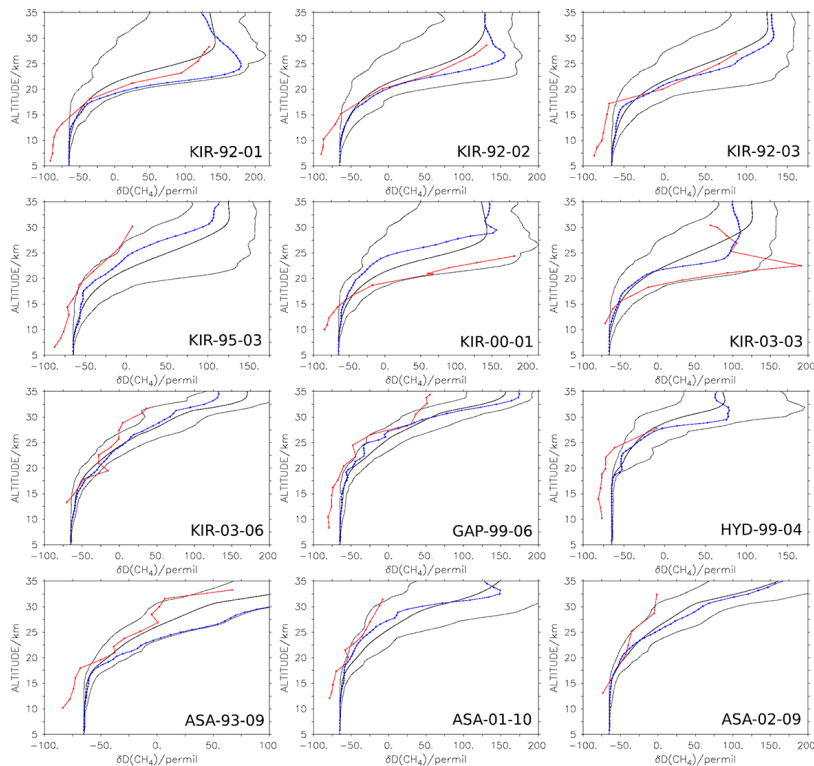
Figure 2. Comparison of $\delta D(CH_4)$ vertical profiles between EMAC and balloon borne data by Röckmann et al. (2011). The red lines show the observations and the blue lines show the EMAC data of the same day at the location of the balloon launch. The black lines represent the simulated averages, minima and maxima of the 21 monthly averages of the respective month at the location of the balloon launch. The flight IDs, included in the panels denote the location, the year and the month of the balloon flight. KIR: Kiruna, Sweden (67.9° N, 21.10° E); GAP: Gap, France (44.44° N, 6.14° E); HYD: Hyderabad, India (17.5° N, 78.60° E); ASA: Aire sur l'Adour, France (43.70° N, 0.30° W).

Full Screen / Esc

Printer-friendly Version

Interactive Discussion
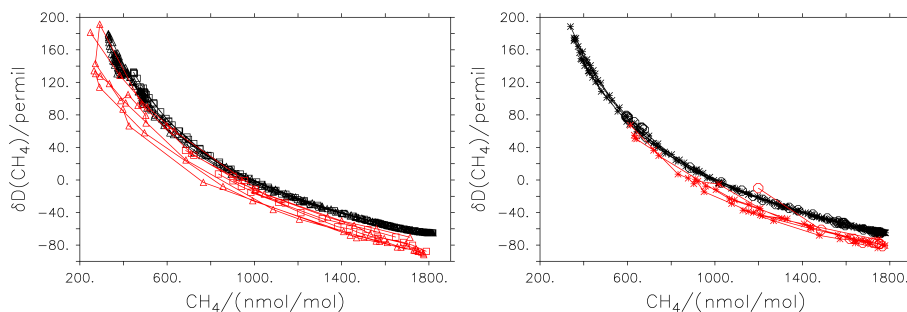
Figure 3. Comparison of the relations of $\delta D(CH_4)$ to CH_4 between EMAC (black) and balloon borne data (red; data as in Fig. 2). The left panel shows the Arctic samples (KIR, $\triangle$: vortex, $\square$: non-vortex) and the right panel shows the mid-latitude ($\ast$) and tropical samples ($\circ$). The altitude range is 5 to 35 km.
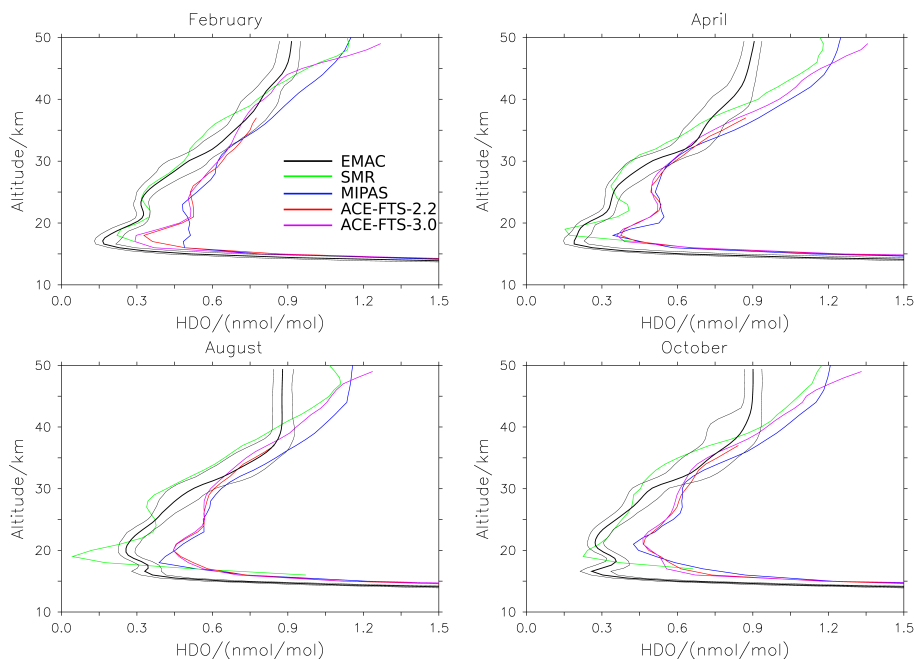
Figure 4. Comparison of HDO mixing ratio-altitude profiles between EMAC and various satellite observations. Black: Averages, minima and maxima of 21 monthly averages of the EMAC simulation for the respective months; green: Odin/SMR; blue: ENVISAT/MIPAS; red: SCISAT/ACE-FTS-2.2; purple: SCISAT/ACE-FTS-3.0.
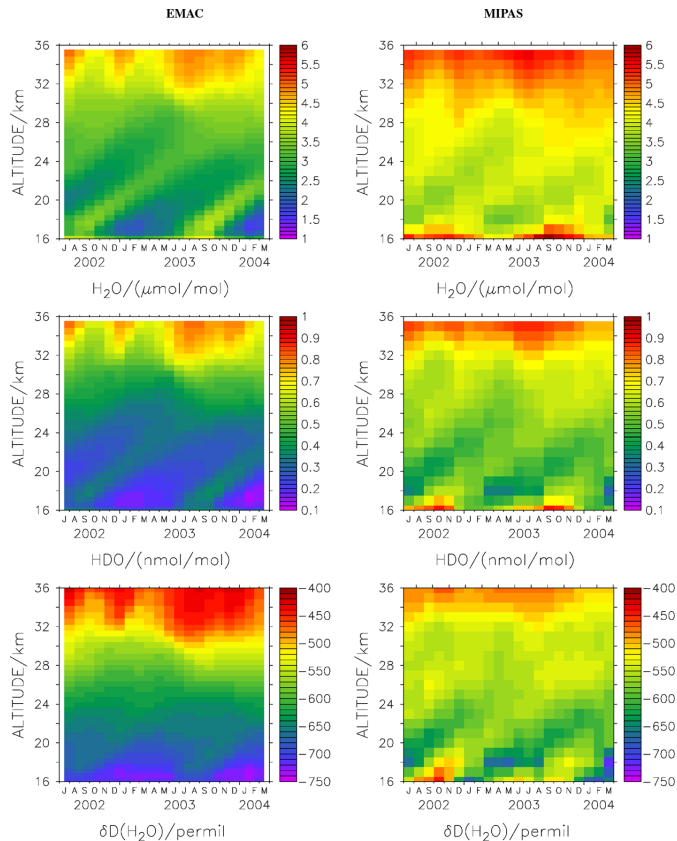
Figure 5. Altitude-time diagrams of H_2O, HDO and $\delta D(H_2O)$ in the tropics (15° S–15° N). Left: EMAC simulation, right: MIPAS observations.

ACPD

14, 23807–23846, 2014

Simulation of the isotopic composition of stratospheric water vapour – Part 1

R. Eichinger et al.

Title Page

Abstract | Introduction

Conclusions | References

Tables | Figures

|◄ | ►|

◄ | ►

Back | Close

Full Screen / Esc

Printer-friendly Version

Interactive Discussion

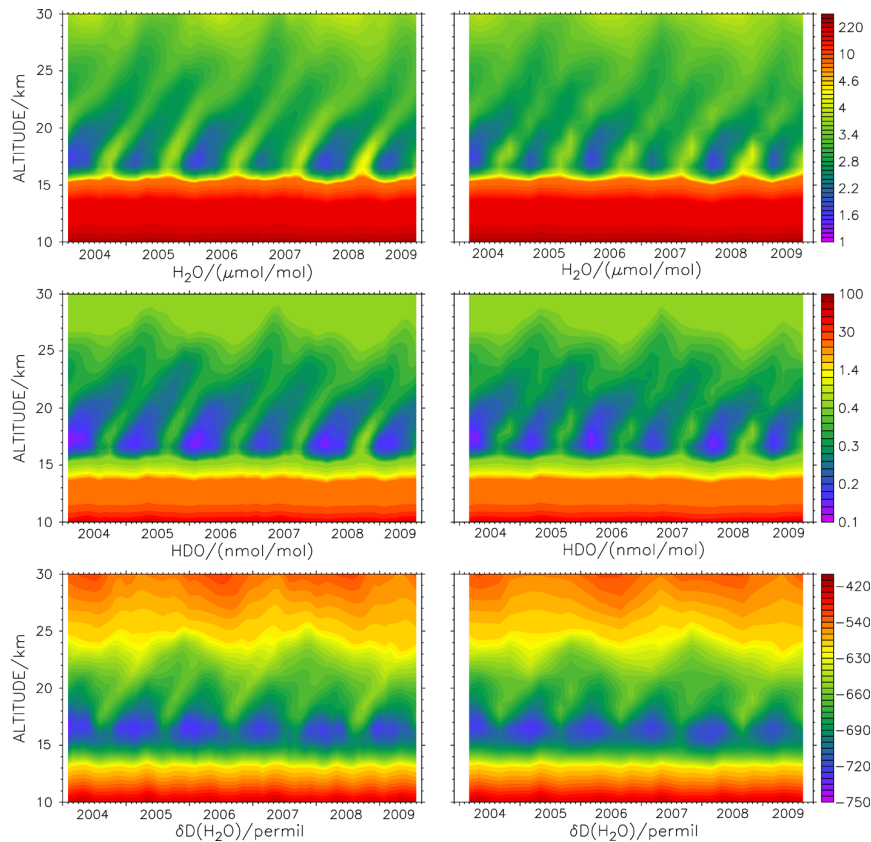**Figure 6.** Altitude-time diagrams of H_2O, HDO and $\delta D(H_2O)$ in the tropics (15° S–15° N) from the EMAC simulation. Left: monthly averages; right: averages of only February, April, August and October, as in Randel et al. (2012). The plotting algorithm linearly interpolates between the available months.